

CamoNAS: Neural Architecture Search for Enhanced Camouflaged Object Detection

Dawei Ren^{1,2*}, Yan Zhang^{1,2}, Hongying Tang^{1,2},
Qiaoling Zhou^{1,3}, Jianpo Liu^{1,2}

¹*Science and Technology on Micro-system Laboratory, Shanghai Institute of Microsystem and Information Technology, Chinese Academy of Sciences, 865 Changning Road, Shanghai, 200050, China.

²University of Chinese Academy of Sciences, No. 19(A) Yuquan Road, Shijingshan District, Beijing, 100049, Beijing, China.

³School of Information Science and Technology, ShanghaiTech University, Shanghai, China.

*Corresponding author(s). E-mail(s): rendawei23@mails.ucas.edu.cn;
Contributing authors: zhangyan232@mails.ucas.ac.cn;
tanghy@mail.sim.ac.cn; zhouql2023@shanghaitech.edu.cn;
liujp@mail.sim.ac.cn;

Abstract

Camouflaged Object Detection (COD) aims to locate and segment objects that blend into their surroundings, presenting challenges due to weak edge cues and ill-defined boundaries. Traditional COD models rely on hand-designed architectures and multi-scale feature fusion, which are often guided by intuition rather than systematic search. This paper introduces CamoNAS, a frequency-aware multi-resolution Neural Architecture Search (NAS) framework for COD. CamoNAS automatically searches both cell-level operations and network-level downsampling paths, forming a hierarchical search space tailored to detect camouflaged objects. Additionally, it adopts an RGB frequency dual-stream architecture, where a learnable wavelet transform complements the RGB spatial stream. CamoNAS achieves state-of-the-art performance on four COD benchmarks (CAMO, COD10K, NC4K, CHAMELEON), highlighting the effectiveness of NAS for COD. Our code is available at <https://github.com/rendaweiSIMIT/CamoNAS>.

Keywords: Camouflaged Object Detection, Neural Architecture Search, Concealed Object Segmentation

1 Introduction

Camouflaged Object Detection (COD) aims to locate and segment objects that blend into their surroundings [1]. It has applications in wildlife conservation [2, 3], medical imaging [4, 5], transparent object detection [6, 7], etc. Compared with conventional detection or segmentation, COD is more challenging because camouflaged targets often mirror the background’s texture, color, and shape, leaving weak edge/gradient cues and ill-defined object-background boundaries. This setting demands precise boundary modeling and strong suppression of background distractors. In recent years, researchers have proposed many architectures and feature-extraction strategies, e.g. mimic human vision [8–10], attention mechanisms [11–13], frequency-domain cues [14, 15], and joint learning with auxiliary vision tasks [16–21]. Collectively, these directions alleviate COD’s difficulty and achieve notable success across diverse scenarios.

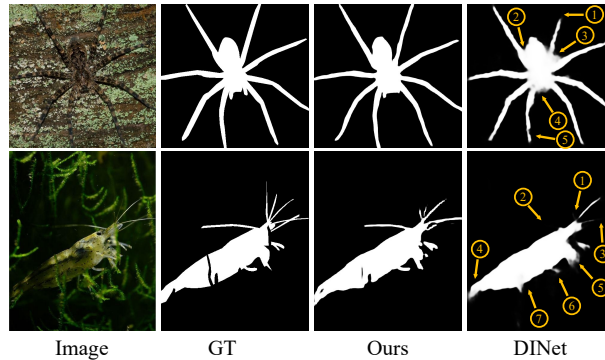


Fig. 1: Qualitative comparison on camouflaged object detection. Under severe foreground–background similarity, the state-of-the-art COD baseline DINet exhibits background leakage, blurred edges, and missing thin structures (orange arrows). Our CamoNAS suppresses these distractions and preserves fine details, producing cleaner masks and sharper contours.

However, most of the above methods rely on manually designed architectures, which require extensive trial-and-error with different network structures and hyperparameter combinations for each dataset or scenario. This process is not only time-consuming and labor-intensive, but it also risks getting stuck in local optima due to human bias, making it difficult to fully explore the vast space of possible model architectures. Neural Architecture Search (NAS) [22] is an automated model design paradigm that has achieved remarkable results in tasks such as image classification [23–27] and semantic segmentation [28–31]. NAS can automatically select network modules and connections from a large candidate search space [32], achieving an excellent trade-off between performance and model complexity. This capability provides a new perspective on how to design deep network structures. However, NAS for COD remains relatively underexplored. Recent work [33] has demonstrated the feasibility of applying NAS to COD, while it remains open how to design COD-specific search

spaces and strategies that jointly ensure precise boundary delineation and robust background suppression [34]. COD places stricter demands on precise boundary delineation and robust suppression of background distractions, leaving unresolved how to tailor the NAS search space and strategy to COD-specific requirements and how to automatically synthesize architectures truly suited to this task.

To address these challenges, we propose CamoNAS, a frequency-aware, multi-resolution NAS framework for COD. CamoNAS is designed to ease the burden of manual network design. Specifically, we build a hierarchical search space ranging from cell-level operator choices to network-level multi-scale path configurations. This design allows the model to dynamically adjust the feature-map resolution at each layer. High spatial resolutions capture fine edges and texture details, whereas low spatial resolutions encode abstract global semantics. In this way, the network satisfies both detail and semantic requirements for COD. Meanwhile, inspired by prior wavelet-like decomposition for COD (e.g., FEDER [15]) and the effectiveness of frequency-domain cues [35, 36], we introduce an LDWT that decomposes the input into four sub-bands (one low-frequency and three directional high-frequency maps) to form a parallel frequency stream alongside the RGB stream. With this RGB-frequency dual-stream architecture, the network can extract discriminative cues from both the spatial domain and the frequency domain separately before fusing them at a high semantic level. This design helps uncover subtle target textures and structural patterns that are hidden in complex backgrounds. In the decoding stage, we adopt a lightweight fusion head based on low-rank matrix decomposition [37] to adaptively fuse the multi-scale features from both streams. This fusion module integrates cross-domain, multi-scale features while preserving key details, thereby reducing semantic conflicts and suppressing background noise. Collectively, these innovations enable CamoNAS to jointly achieve precise boundary delineation and accurate whole-object localization for camouflaged targets, thereby delivering significant improvements in segmentation accuracy and robustness under challenging camouflage.

In summary, our approach combines automated NAS-based modeling with COD-specific design considerations, producing high-performance COD models without tedious manual tuning. Our main contributions are as follows:

- We propose a NAS framework tailored to COD, with a hierarchical search space spanning cell-level operators and network-level cross-scale routing, enabling end-to-end architecture optimization for camouflaged targets.
- We incorporate a learnable wavelet-based frequency decomposition module into NAS to form an RGB-frequency dual-stream network. The module produces four sub-bands (one low-frequency and three directional high-frequency components) and is trained with an explicit perfect-reconstruction regularization, providing complementary texture and structural cues for COD.
- We achieve competitive state-of-the-art performance on four benchmark COD datasets across all standard metrics, and comprehensive experiments, including ablation studies, confirm the effectiveness of our technique.

2 Related Work

2.1 Camouflaged Object Detection

In COD tasks, the core difficulty is the high intrinsic similarity between foreground and background, which makes targets blend seamlessly into their surroundings [38–41]. To counter this, prior work enhances target cues while suppressing background noise. Representative designs include symmetric/multi-scale fusion (SINet) [1] for edge delineation, hard-region mining with residual fusion (PFNet) [9], joint learning with saliency for contrast-aware localization, edge-guided supervision for complete structures (BGNet) [17], and multi-scale zoom-in/zoom-out reasoning (ZoomNet) [10]. Frequency cues have also been introduced: learnable wavelet decomposition to expose textural signals, and masked separable attention to refine multi-level aggregation (CamoFormer) [42].

Beyond these frequency-aware designs, recent COD models further improve performance by refining global–local fusion and iterative decoding. Yue *et al.* [43] fuse convolutional and Vision Transformer representations at the decision level to couple global context with fine-grained details for camouflaged object segmentation, while Ge *et al.* [44] propose a feature-aware iterative refinement network that progressively recovers complete camouflaged objects via feature- and edge-aware refinement. These advances have improved results on *CHAMELEON* [45], *CAMO* [41], *COD10K* [1], and *NC4K* [19]. Yet most methods—including recent CNN–ViT hybrids and iterative refinement frameworks—rely on hand-crafted architectures and empirical tuning [2, 4, 46], limiting generalization across datasets and scenes. A recent survey [34] further highlights persistent gaps in fine detail reconstruction and robustness. This motivates automated architecture optimization, which is the direction we pursue.

Despite rich feature-extraction [47, 48] and context-fusion strategies [49, 50], balancing fine-grained boundaries with global semantics remains challenging. Many designs employ deep fusion, attention, or auxiliary heads (e.g., boundary/saliency) [17–21], often increasing complexity without consistent cross-domain generalization. Beyond COD, transformer architectures based on mutual attention for image anomaly detection [51], dual-branch Swin Transformer–ConvNeXt networks for strong-noise image denoising [52], and robust segmentation under label noise for 3D point clouds [53] further demonstrate the importance of expressive yet robust multi-branch and multi-scale representations under challenging supervision. We therefore introduce NAS for COD to obtain end-to-end, data-driven architectures that reduce manual effort and improve robustness in varied camouflage scenarios.

2.2 Neural Architecture Search for Semantic Segmentation

NAS [22] automates topology and operator selection and has shown strong results in classification [23–27, 54], detection [24, 55–57], and segmentation [28–31]. Early RL/evolutionary NAS [23, 58] are computationally expensive; differentiable relaxation methods, pioneered by DARTS [32] and its variants [59–61], convert discrete architectural choices into learnable weights, thereby enabling efficient gradient-based search with significantly reduced computational cost. More recently, one-shot NAS

frameworks such as MNGNAS distill adaptive combinations of multiple searched sub-networks into a single supernet, improving both search stability and final accuracy [62].

Extending NAS to dense prediction raises memory and multi-scale representation challenges [22], but notable successes exist: NAS-FPN [63] discovers superior feature pyramids, MnasNet [64] optimizes accuracy–latency for mobile via device-aware objectives, and EfficientDet [65] couples BiFPN with compound scaling for strong COCO performance. Other variants improve practicality—ProxylessNAS [66] performs direct, target-task search without proxies, while progressive strategies [25] accelerate exploration. In parallel, efficient attention pyramid transformers, such as EAPT [67], demonstrate that carefully designed multi-scale attention can benefit image classification, object detection, and semantic segmentation, reinforcing the importance of hierarchical global–local modeling within the search space.

Collectively, these works show that NAS and attention-based backbones can find architectures that outperform hand-crafted baselines while balancing accuracy and complexity [32, 68–70]. Beyond general dense prediction, recent work has also brought NAS into COD. Li *et al.* propose ALRNet [33], which searches camouflage-specific modules for coarse localization and edge-assisted refinement. Building on this line of research, we explore a complementary direction: CamoNAS jointly searches macro-level multi-resolution routing (down/hold/up) together with cell-level operators, and further integrates a learnable wavelet-based frequency stream into the NAS process to derive frequency-aware architectures for sharper boundaries and stronger generalization in camouflage scenes.

3 Methodology

Motivation.

Motivated by the limited design space and heavy tuning burden of hand-designed networks [22], we pursue NAS-driven topology discovery for COD. We replace manual heuristics with an automatically searched topology: a differentiable, resolution-aware NAS that co-optimizes cell operators and down/hold/up paths. In parallel, a learnable discrete wavelet transform forms a frequency stream that complements the RGB stream, and a lightweight late-fusion head aggregates both. This design allocates capacity across sub-bands and resolutions, sharpening edges and suppressing distractors without heavy hyperparameter tuning.

3.1 Architecture Overview

As illustrated in Fig. 2, CamoNAS comprises four components: (i) a learnable discrete wavelet transform (LDWT), (ii) two NAS-searched backbones (an RGB stream and a frequency stream), (iii) a network-level resolution path search, and (iv) a late-fusion head. The LDWT decomposes the input into one low-frequency map L and three directional high-frequency maps $\{H, V, D\}$, yielding a 4-channel tensor ($4 \times H \times W$) that feeds the Frequency stream, while the original RGB image ($3 \times H \times W$) feeds the RGB stream. Each stream is organized into four stages operating at spatial scales $S = \{\frac{1}{4}, \frac{1}{8}, \frac{1}{16}, \frac{1}{32}\}$ of $H \times W$; within a stage, differentiable micro-cells update

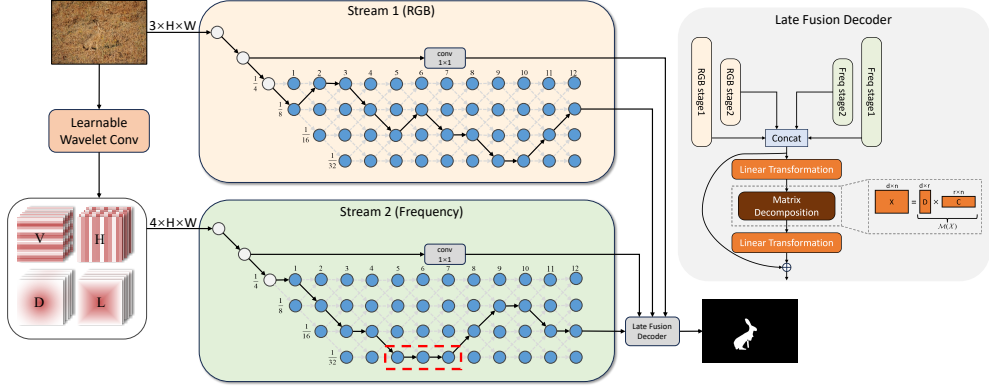


Fig. 2: Overview of CamoNAS. A learnable wavelet convolution (LDWT) splits the image into four sub-bands (L, H, V, D), yielding a $4 \times H \times W$ frequency input that runs in parallel with RGB. The top and bottom backbones are two NAS-searched streams operating at four resolutions ($\frac{1}{4}, \frac{1}{8}, \frac{1}{16}, \frac{1}{32}$ of $H \times W$). Within each stage, blue nodes denote intermediate block states and edges denote candidate operations. At the network level, down/hold/up transitions between adjacent scales are jointly optimized with the cell operations in a single supernet, enabling dynamic multi-resolution paths. Selected multi-scale features from both streams are concatenated and fed to a late-fusion decoder to predict the mask, yielding sharper object boundaries and better detail preservation in camouflaged scenes.

hidden states, where nodes denote block states and edges denote candidate operations. At the network level, down/hold/up transitions between adjacent scales are learned to form dynamic multi-resolution paths. Unlike hand-designed COD networks (e.g., SNet/DINet) that adopt a fixed, monotonic downsampling schedule with pre-defined fusion/refinement modules, CamoNAS learns the routing decisions (down/hold/up) from data and jointly optimizes them with cell structures. During training, we instantiate a supernet that contains all micro-cells and all scale transitions, and jointly optimize network weights and architecture parameters via continuous relaxation. After the final stage, selected features from both streams (e.g., $F_{\text{stage1}}^R, F_{\text{stage2}}^R, F_{\text{stage1}}^F, F_{\text{stage2}}^F$) are concatenated and passed through the *Fusion Head*: a linear mapping, a low-rank matrix decomposition $X \approx DC$, and a second projection that outputs a segmentation mask at the original image size. The entire model is trained with a structure-aware loss [71, 72] to emphasize boundaries and fine details in camouflaged scenes.

3.2 Learnable Wavelet Frequency Decomposition

Existing frequency decomposition schemes rely on fixed filter templates [14, 35, 36] (e.g., Laplacian pyramids, DFT). Their high/low frequency splits and directional responses remain static during training, making it difficult to adapt to varying texture

amplitudes and spatial scales in camouflage scenarios. Moreover, such hard-coded filtering lacks reversibility constraints. In addition, recent COD studies have explored learnable wavelet-like decomposition [15], demonstrating the effectiveness of frequency-aware representations. Motivated by these observations, we implement a learnable discrete wavelet transform as an end-to-end convolutional operator $\mathcal{W}(\cdot; \theta)$, which is updated in sync with the network’s weights and architecture parameters during training.

We use two learnable 1D analysis filters $\mathbf{a}_0, \mathbf{a}_1 \in \mathbb{R}^K$ (each of length K). From these, four separable 2D convolution kernels are formed by outer products:

$$\begin{aligned} F_{ll} &= \mathbf{a}_0 \otimes \mathbf{a}_0^\top & F_{lh} &= \mathbf{a}_0 \otimes \mathbf{a}_1^\top \\ F_{hl} &= \mathbf{a}_1 \otimes \mathbf{a}_0^\top & F_{hh} &= \mathbf{a}_1 \otimes \mathbf{a}_1^\top \end{aligned} \quad (1)$$

The transform performs the forward wavelet transform using a group convolution:

$$X^w = \mathcal{W}(X; \theta) = \{X^L, X_h^H, X_v^H, X_d^H\} \quad (2)$$

The four groups of output features correspond to the low-frequency component, horizontal high-frequency, vertical high-frequency, and diagonal high-frequency components. We implement the dyadic downsampling with a stride-2 group convolution, thus no additional pooling is required. To ensure that the wavelet transform and its inverse form a stable invertible pair early in training, we tie the parameters of the analysis and synthesis filters and impose two perfect reconstruction constraints:

$$\begin{aligned} A_0(z)S_0(z) + A_1(z)S_1(z) &= 2 \\ A_0(-z)S_0(z) + A_1(-z)S_1(z) &= 0 \end{aligned} \quad (3)$$

$A_k(z)$ and $S_k(z)$ are the z^- -transforms of the corresponding filters, which are explicitly regularized in the frequency domain to ensure lossless round trips and suppress aliasing. We incorporate these constraints into the training objective as penalty terms. They add minimal overhead to the training process but significantly improve the network’s ability to preserve high frequency information.

3.3 Hierarchical and Multi-Scale Search

3.3.1 Cell-Level Search

Similar to DARTS-style architectures [32, 59–61], we construct the network as a hierarchy of multiple cells stacked sequentially. Each cell serves as a basic building block and contains several internal blocks. We model a cell as a directed acyclic graph (DAG) and adopt continuous relaxation to enable efficient gradient-based optimization of its discrete structure, facilitating the search over a large architecture space. Below, we detail the design of the cell-level search space. The overall cell-level search space is illustrated in Fig. 3.

Suppose a cell contains n blocks, and let H^i denote the output of the i -th block (for $i = 1, 2, \dots, n$). In each block, we first select two input features from a candidate set C (denote them as I_1 and I_2 as in the diagram). We then apply two operators

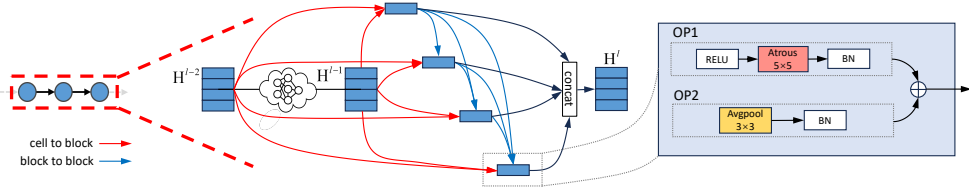


Fig. 3: Cell-level search space of CamoNAS. In the l -th cell, the candidate input set consists of the two preceding cell outputs (H^{l-2} , H^{l-1}) and all earlier block states within the cell (red: cell→block, blue: block→block). Each block selects two inputs $I_1, I_2 \in C$, applies two operators $O_1, O_2 \in \mathcal{O}$ (examples on the right), and outputs $H^i = O_1(I_1) + O_2(I_2)$; edges are weighted by architecture parameters α under continuous relaxation during search. The outputs of all active blocks are concatenated to form the cell output H^l .

O_1 and O_2 to these features respectively, and finally sum the two resulting tensors element-wise to obtain the block's output $H^i = O_1(I_1) + O_2(I_2)$.

Here, O_1 and O_2 are the chosen operations for inputs I_1 and I_2 , respectively, and $I_1, I_2 \in C$ are the two inputs selected from the candidate set C . The candidate input set C is defined as:

$$C = \{H_{\text{cell-1}}, H_{\text{cell-2}}\} \cup \{H^1, H^2, \dots, H^{i-1}\} \quad (4)$$

Specifically, $H_{\text{cell-1}}$ and $H_{\text{cell-2}}$ represent the outputs from the previous and the preceding-to-previous cells, respectively. $\{H^1, \dots, H^{i-1}\}$ denotes the outputs of all internal blocks within the current cell.

For the selected inputs I_1 and I_2 , we separately apply operations O_1 and O_2 for feature transformations. Based on a comprehensive consideration of existing COD research [1], we set our candidate operation set \mathcal{O} to include eight widely used convolutional operations: two depthwise separable convolutions, two atrous convolutions (with dilation $r = 2$), average pooling, max pooling, skip connection, and no connection. These fixed operations enhance feature extraction capabilities from multiple perspectives while maintaining computational simplicity. Moreover, inspired by recent frequency-sensitive filters commonly accelerated via GPU [73, 74], we incorporate directional edge filters (Sobel), Haar wavelet split, and Gaussian blur to further enhance the model's capacity in capturing edge targets. Given that depthwise separable convolutions have been proven sufficient to serve as parameter-efficient benchmarks in recent NAS research, we no longer separately include ordinary convolution, thus maintaining conciseness of the search space. Additionally, by combining fixed operations with learnable components, we maintain simplicity while expanding the versatility of operations. Such a design ensures stable dimensionality and consistent gradient flow. The final output of each cell H_{cell} is obtained by concatenating the outputs of all blocks along the channel dimension, as follows:

$$H_{\text{cell}} = \text{Concat}_{\text{channel}}(H^1, H^2, \dots, H^i) \quad (5)$$

During the search process, we adopt a continuous relaxation strategy for the candidate operations, converting discrete operation choices into learnable continuous parameters. Specifically, for each candidate operation o in operation set O , we introduce a parameter α_o . After applying a softmax normalization, the output for the j -th input I_j in the i -th block is computed as a weighted sum of all candidate operations:

$$O_j(I_j) = \sum_{o \in O} \frac{\exp(\alpha_o)}{\sum_{o' \in O} \exp(\alpha_{o'})} \cdot o(I_j) \quad (6)$$

Such continuous relaxation not only enables differentiable cell-level search, but also allows us to leverage gradient-based optimization to update the architecture parameters end-to-end, progressively exploring candidate architectures that fulfill task-specific requirements from coarse to fine levels.

3.3.2 Layer-level Search

Based on the constructed cell-level search space, we further design the overall network architecture consistent with the multi-resolution search strategy adopted in micro-architecture-level searches. The network consists of multiple stacked cells, dynamically adjusting the spatial resolution of feature maps between layers to meet the dual demands of fine-grained edge detection and global semantic comprehension. In our design, the initial network front end adopts two layers of convolution for preliminary feature extraction and downsampling, producing initial hierarchical features. Then, the network comprises L cells, each layer $l \in \{1, \dots, L\}$ operating at four discrete resolutions:

$$S = \left\{ s_1 = \frac{1}{4}, s_2 = \frac{1}{8}, s_3 = \frac{1}{16}, s_4 = \frac{1}{32} \right\} \quad (7)$$

where each cell explicitly searches its resolution paths and cross-layer information flow.

To ensure continuity of spatial resolution across layers, we impose strict constraints on the resolution transitions between layers. Specifically, the state of layer l can only be derived from states of the preceding layer ($l - 1$) through $\{\times 1, \times 2, \times \frac{1}{2}\}$ scaling operations:

$$s^l \in \left\{ s^{l-1}, 2s^{l-1}, \frac{1}{2}s^{l-1} \right\} \cap S \quad (8)$$

The highest resolution is fixed at $s_1 = \frac{1}{4}$, and the lowest resolution is $s_4 = \frac{1}{32}$.

To introduce differentiability into discrete paths, for layer l , we define a learnable parameter $\beta_{s \rightarrow s'}^l$ for transitions from scale s to s' . Through softmax normalization, we obtain transition probabilities:

$$\pi_{s \rightarrow s'}^l = \frac{\exp(\beta_{s \rightarrow s'}^l)}{\sum_{s'' \in N(s)} \exp(\beta_{s \rightarrow s''}^l)} \quad (9)$$

Where $N(s) = \{s, 2s, \frac{1}{2}s\} \cap S$. During forward propagation, the hidden state at scale s for layer $l - 1$ is denoted as \mathbf{H}_s^{l-1} . It is mapped to the target scale s' through

upsampling or downsampling operators (bilinear interpolation), denoted as: $R(s \rightarrow s')$ and subsequently passed into the current cell:

$$\tilde{\mathbf{H}}_{s'}^l = \sum_{s \in N(s')} \pi_{s \rightarrow s'}^l R(s \rightarrow s') (\mathbf{H}_s^{l-1}) \quad (10)$$

The inputs $\tilde{\mathbf{H}}_{s'}^l$ at various resolutions are collectively fed into the l -th cell, yielding new hidden states $\mathbf{H}_{s'}^l$. This iterative approach jointly optimizes resolution paths and cell-internal operation selection.

In summary, the layer-level search learns when to keep, upsample, or downsample, producing data-driven multi-resolution paths instead of a fixed schedule. This lets high-resolution features preserve fine boundaries while low-resolution features consolidate global semantics in a complementary way. The resulting multi-scale states feed directly into the RGB-frequency fusion, enabling accurate camouflaged-object segmentation with modest complexity.

3.4 Fusion Head

In the previous sections, we have separately exploited rich multi-scale features from RGB and frequency-domain streams via Cell-NAS units. However, effectively integrating these cross-domain and cross-layer features remains challenging because direct concatenation often introduces information redundancy and semantic inconsistency between high- and low-level features, which degrades precise segmentation of camouflaged objects [1]. Therefore, we adopt a lightweight decoding module, designed as a low-dimensional embedding-based decoder. The Fusion Head adaptively integrates features while preserving key details and suppressing noise simultaneously.

Specifically, we first resize all selected features to the same spatial resolution, align channels with 1×1 projections, and flatten spatial dimensions so that $n = H \times W$. We then define:

$$X = \text{Concat}(F_{\text{stage1}}^R, F_{\text{stage2}}^R, F_{\text{stage1}}^F, F_{\text{stage2}}^F) \quad (11)$$

To effectively merge these multi-stage features, the Fusion Head applies a linear projection Φ_1 to obtain a compact embedding with a common channel size d :

$$Z = \Phi_1(X) \in \mathbb{R}^{d \times n} \quad (12)$$

The embedding is then factorized by a low-rank module:

$$Z \approx DC \quad D \in \mathbb{R}^{d \times r} \quad C \in \mathbb{R}^{r \times n}, \quad r \ll d \quad (13)$$

We employ a soft vector quantization (Soft-VQ) [75] scheme to obtain a low-rank approximation. Soft-VQ first computes cosine scores between dictionary atoms and column features:

$$s_{ij} = \frac{d_i^\top z_j}{\|d_i\| \|z_j\|} \quad i = 1, \dots, r, \quad j = 1, \dots, n \quad (14)$$

Membership weights are obtained via a temperature-controlled softmax over atoms:

$$C_{ij} = \frac{\exp(s_{ij}/T)}{\sum_{k=1}^r \exp(s_{kj}/T)} \quad (15)$$

The compact embedding is then reconstructed as $\hat{Z} = DC$. A second linear projection Φ_2 restores channels and forms a residual with Z :

$$Y = \Phi_2(\hat{Z}) + Z \quad (16)$$

Finally, after reshaping Y back to feature maps, BatchNorm and a two-layer 1×1 MLP produce the segmentation mask M ; when the decoder operates at a reduced scale, we apply bilinear upsampling to match the original image resolution.

3.5 Search and Training Strategy

The optimization procedure of CamoNAS is divided into two sequential stages [68]. The first stage jointly optimizes the network topology (cell operators and multi-resolution routing) while learning the LDWT kernels end-to-end. The second stage retrains weights on the discretized final architecture. The entire process maintains end-to-end differentiability. Specifically, the internal operations within each cell are probabilistically controlled by α , cross-layer resolution transitions by β , learnable wavelet kernels by θ , and ordinary convolution and normalization parameters by ω .

Architecture Search Stage: In the joint search stage, continuous relaxation is adopted, where parameters α and β after softmax normalization directly propagate forward; parameters ω and θ directly parameterize weights. We define the task loss as $L_{seg}(\omega, \theta; \alpha, \beta)$, along with a wavelet completeness regularization:

$$L_{wavelet}(\theta) = \sum_{k=0}^{N-1} \left(\langle a_0, s_0 \rangle_k + \langle a_1, s_1 \rangle_k - \hat{V}_k \right)^2 \quad (17)$$

We then iteratively update parameters (ω, θ) on the training subset D_{trainA} and update (α, β) on the validation subset D_{trainB} :

$$(\omega, \theta) \leftarrow (\omega, \theta) - \eta_\omega \nabla_{\omega, \theta} [L_{seg} + \lambda L_{wavelet}] \quad (18)$$

$$(\alpha, \beta) \leftarrow (\alpha, \beta) - \eta_\alpha \nabla_{\alpha, \beta} L_{seg} \quad (19)$$

Here, η_ω and η_α use shared cosine annealing schedules. To avoid premature fluctuations, we freeze α, β for the first T_0 epochs and optimize only the network weights (ω, θ) .

Discretization and Retraining Stage: After completing the search, for each cell, the discretized architecture \hat{a} is obtained by taking the argmax over softmax weights. For network-level discretization, the optimal path $\hat{\beta}$ is solved via Viterbi decoding on the layer-scale resolution probability map. After discretization, parameters θ^* are

locked, and comprehensive retraining on the entire dataset is initiated. The total loss at this stage is:

$$L_{total}(x, y) = L_{struct}(x, y) + \lambda L_{wavelet}(\theta^*) \quad (20)$$

Where L_{struct} maintains the structure-aware BCE+IoU form [71, 72], and $L_{wavelet}$ merely serves as a constant regularizer for determined wavelet kernels, no longer impacting gradient updates. This two-stage strategy allows sufficient exploration of α, β during the search stage and ensures that θ does not degenerate after discretization. Consequently, the obtained network effectively exploits complementarity between RGB and frequency-domain streams, significantly improving segmentation accuracy on object boundaries and fine details.

4 Experiments

4.1 Training Settings

To ensure reproducibility and fairness, we strictly follow widely accepted NAS experimental setups [14, 15], dividing training into architecture search and final-model retraining.

Architecture Search Stage. The training dataset is randomly split into two equally sized subsets D_{train}^A and D_{train}^B , each containing 2020 images. Network weights (ω, θ) are updated on D_{train}^A . Architecture parameters (α, β) are updated using Adam on D_{train}^B with an initial learning rate of 3×10^{-4} , for 60 epochs with batch size 2. Both architecture and weight optimizers use cosine-annealing schedules. We empirically observed that updating the architecture parameters (α, β) from the outset often traps the search in local optima. Accordingly, we adopt a warm-up schedule that optimizes only the network/LDWT weights (ω, θ) for the first 20 epochs before enabling updates to (α, β) ; the full search used 4 GPU-days on two NVIDIA RTX 2080 Ti GPUs.

Discretization and Retraining Stage. After the search, we retrain the discretized architecture from scratch on the full training set for 90 epochs with SGD (initial LR 1×10^{-3} ; step decay $\times 0.5$ every 20 epochs; momentum 0.9; weight decay 1×10^{-5} ; batch size 16).

All training images are resized and randomly cropped to 512×512 , with random horizontal flipping, scale jitter (0.8-1.2 \times), and color jitter for data augmentation [2, 3]. Our implementation is in PyTorch and runs on two NVIDIA RTX 2080 Ti GPUs.

4.2 Datasets

To rigorously evaluate the generalization and robustness of our model, we conduct experiments on four widely adopted benchmark datasets for COD, including *CHAMELEON*, *CAMO*, *COD10K*, and *NC4K*. Following the official splits used in prior works [10] to ensure an unbiased comparison, we train on 1,000 images from *CAMO* and 3,040 images from *COD10K*. The testing phase is conducted on the full testing subsets of the datasets mentioned above, ensuring comprehensive and balanced performance evaluation across diverse scenarios.

Methods	Pub.	CHAMELEON				CAMO				COD10K				NC4K			
		$M \downarrow$	$F_\beta^\omega \uparrow$	$E_\phi \uparrow$	$S_\alpha \uparrow$	$M \downarrow$	$F_\beta^\omega \uparrow$	$E_\phi \uparrow$	$S_\alpha \uparrow$	$M \downarrow$	$F_\beta^\omega \uparrow$	$E_\phi \uparrow$	$S_\alpha \uparrow$	$M \downarrow$	$F_\beta^\omega \uparrow$	$E_\phi \uparrow$	$S_\alpha \uparrow$
SAM [76]	—	0.207	0.595	0.647	0.635	0.160	0.597	0.639	0.643	0.093	0.673	0.737	0.730	0.118	0.675	0.723	0.717
SAM-S [76]	—	0.076	0.729	0.820	0.650	0.105	0.682	0.774	0.731	0.046	0.695	0.828	0.772	0.071	0.747	0.832	0.763
SINet [2]	CVPR20	0.034	0.806	0.938	0.872	0.092	0.644	0.804	0.745	0.043	0.631	0.864	0.776	0.058	0.723	0.871	0.808
JSCOD [77]	CVPR21	0.030	0.848	0.943	0.894	0.073	0.728	0.859	0.800	0.035	0.684	0.884	0.809	0.047	0.771	0.898	0.842
PFNet [9]	CVPR21	0.033	0.810	0.921	0.882	0.085	0.695	0.841	0.782	0.040	0.660	0.877	0.800	0.053	0.745	0.887	0.829
FDNet [14]	CVPR22	0.030	0.819	0.948	0.894	0.063	0.775	0.895	0.841	0.030	0.729	0.919	0.840	0.052	0.750	0.893	0.834
SegMaR [20]	CVPR22	0.027	0.835	0.950	0.897	0.071	0.753	0.874	0.815	0.034	0.724	0.899	0.833	0.046	0.781	0.896	0.841
ZoomNet [10]	CVPR22	0.023	0.845	0.943	0.902	0.066	0.752	0.877	0.820	0.029	0.729	0.888	0.838	0.043	0.784	0.896	0.853
DGNet [78]	MIR23	0.029	0.816	0.934	0.890	0.057	0.769	0.901	0.839	0.033	0.693	0.896	0.822	0.042	0.784	0.911	0.857
PopNet [79]	ICCV23	0.022	0.893	0.962	0.910	0.077	0.744	0.859	0.808	0.028	0.757	0.910	0.851	0.042	0.802	0.910	0.861
FEDER [15]	CVPR23	0.028	0.855	0.947	0.894	0.069	0.785	0.873	0.807	0.032	0.740	0.900	0.823	0.045	0.817	0.905	0.846
SCOD [80]	AAAI23	0.046	0.791	0.897	0.818	0.092	0.709	0.815	0.735	0.049	0.637	0.832	0.733	0.064	0.751	0.853	0.779
WS-SAM [81]	NeurIPS24	0.046	0.777	0.897	0.824	0.090	0.716	0.818	0.759	0.038	0.719	0.878	0.803	0.052	0.802	0.886	0.829
ICEG [82]	ICLR24	0.027	0.858	0.950	0.899	0.068	0.789	0.879	0.810	0.030	0.747	0.906	0.826	0.044	0.814	0.908	0.849
DINet [83]	TMM24	-	-	-	-	0.063	0.775	0.895	0.841	0.030	0.729	0.919	0.840	0.052	0.750	0.893	0.834
ZoomNeXt [84]	TPAMI24	0.020	0.863	0.969	0.912	0.069	0.760	0.885	0.822	0.026	0.758	0.926	0.855	0.038	0.808	0.925	0.869
GenSAM [85]	AAAI24	0.090	0.680	0.807	0.764	0.113	0.659	0.775	0.719	0.067	0.681	0.838	0.775	-	-	-	-
DINO [86]	CVPR25	0.031	0.825	0.931	0.864	0.077	0.747	0.862	0.793	0.031	0.763	0.916	0.834	0.043	0.818	0.923	0.850
CIRCOD [87]	WACV25	-	-	-	-	0.063	0.772	0.894	0.824	0.030	0.741	0.916	0.835	0.040	0.808	0.920	0.858
Ours	—	0.023	0.904	0.966	0.911	0.062	0.808	0.902	0.831	0.027	0.798	0.926	0.853	0.041	0.827	0.918	0.858

Table 1: Results on COD. The best three results are highlighted in **red**, **green** and **blue**.

4.3 Evaluation Metrics and Comparison

We evaluate COD with four standard metrics: structure measure (S_α), mean absolute error (MAE, M), weighted F-measure (F_β^ω) and mean E-measure (E_ϕ). We compare CamoNAS with over ten representative methods (e.g., SINet, JSCOD, PFNet, FDNet, SegMaR, ZoomNet, DGNet, DINet) on *CHAMELEON*, *CAMO*, *COD10K*, and *NC4K*. For fairness, predictions for baselines are obtained from official releases or reproduced from their public code under the same protocols.

4.4 Experimental Results

Quantitative. Table 1 summarizes results on *CHAMELEON*, *CAMO*, *COD10K*, and *NC4K*. CamoNAS surpasses strong baselines (e.g., DINet, PopNet) on most metrics and datasets, delivering strong overall performance across M , F_β^ω , E_ϕ , and S_α , with especially notable gains on *CHAMELEON* and *COD10K*.

Qualitative. Fig. 4 shows representative cases from *CHAMELEON*, *CAMO*, *COD10K*, and *NC4K*. The panel spans typical COD challenges small or huge targets, multiple instances, occlusion, and boundary uncertainty. CamoNAS recovers finer structures and boundaries while better suppressing cluttered backgrounds, highlighting robustness under diverse camouflage scenarios.

4.5 Ablation Study and Analysis

For a fair comparison, all variants are trained and evaluated under the same codebase, schedules, and augmentations. Unless otherwise stated, we train on *CAMO* (1,000 images) and *COD10K* (3,040 images), and report results on COD10K-Test (2026 images). All runs are conducted on two NVIDIA RTX 2080 Ti GPUs with identical hyper-parameters. We ablate one factor at a time and report M , F_β^ω , E_ϕ , and S_α .

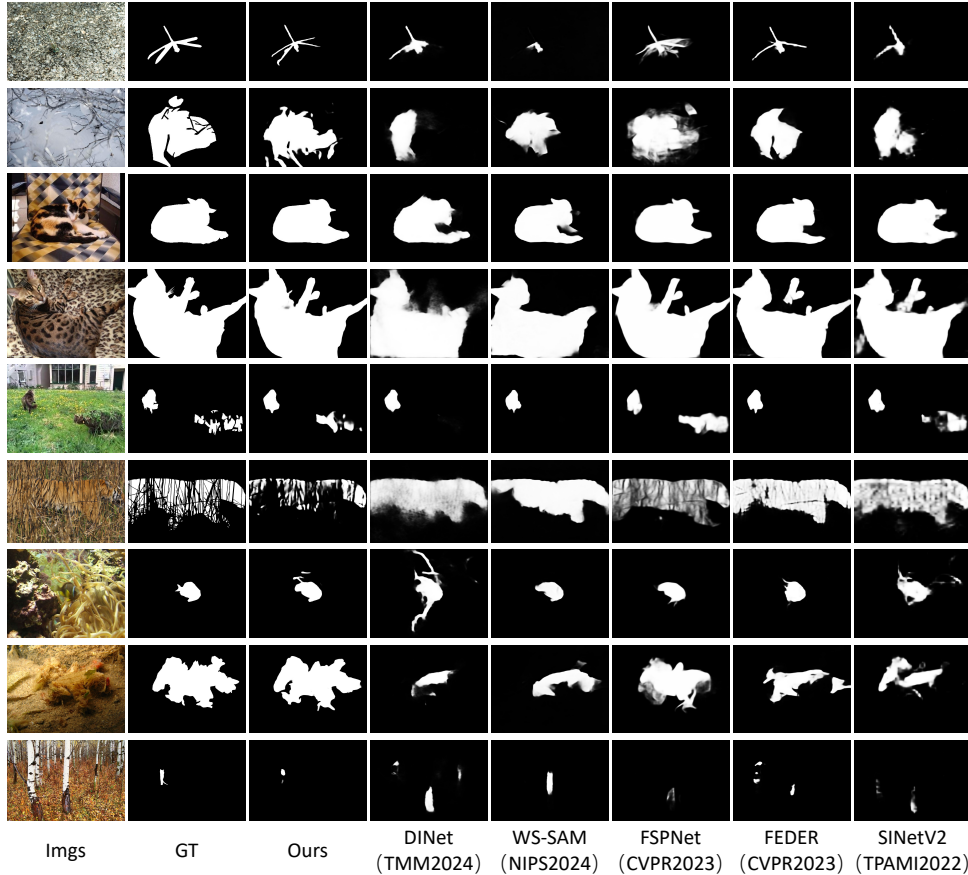


Fig. 4: Qualitative comparisons of our CamoNAS with state-of-the-art methods.

Dual-stream frequency modeling. Adding a frequency branch to the RGB stream consistently improves performance across benchmarks (Table 2a). LDWT stabilizes sub-band decomposition, and a mild wavelet regularizer L_{wav} further helps by preserving informative high/low-frequency structure.

Operator space \mathcal{O} . Expanding $\mathcal{O}_{\text{base}}$ with Sobel, HaarSplit, and Gaussian yields consistent but modest gains (Table 2b), serving as a generic low-level operator vocabulary. Notably, NAS still determines whether and where to use these primitives across edges/stages/scales. Compared with operator enrichment (Table 2b), replacing the searched cross-scale routing leads to a much larger drop (Table 2c), indicating that the main improvement comes from routing/topology discovery rather than the operators alone.

Cross-scale path search. Fixed single-scale or fixed four-scale schedules underuse cross-scale complementarity, and greedy routing is often locally optimal (Table 2c). Jointly searching down/hold/up transitions attains stronger structure-aware alignment while keeping MAE competitive. This controlled comparison indicates that the

RGB	Freq	LDWT	L_{wav}	$M \downarrow$	$F_{\beta}^{\omega} \uparrow$	$E_{\phi} \uparrow$	$S_{\alpha} \uparrow$	$\mathcal{O}_{\text{base}}$	Sobel	HaarSplit	Gaussian	$M \downarrow$	$F_{\beta}^{\omega} \uparrow$	$E_{\phi} \uparrow$	$S_{\alpha} \uparrow$
✓				0.083	0.552	0.748	0.690	✓				0.037	0.755	0.892	0.824
✓	✓			0.052	0.641	0.834	0.753	✓	✓			0.033	0.752	0.904	0.822
✓	✓	✓		0.039	0.726	0.887	0.805	✓	✓	✓		0.030	0.776	0.913	0.840
✓	✓	✓	✓	0.027	0.798	0.926	0.853	✓	✓	✓	✓	0.027	0.798	0.926	0.853

(a) Dual-Stream Frequency Modeling

Metrics	Concat+1×1	Hamburger [75]	Soft-VQ ($r=16$)	Soft-VQ ($r=32$, ours)
$M \downarrow$	0.049	0.039	0.031	0.027
$F_{\beta}^{\omega} \uparrow$	0.665	0.708	0.774	0.798
$E_{\phi} \uparrow$	0.847	0.878	0.915	0.926
$S_{\alpha} \uparrow$	0.762	0.795	0.835	0.853

(b) Operation Space \mathcal{O}

Metrics	Fixed 1/8	Fixed 1/16	Fixed 4-scale	Greedy	Ours
$M \downarrow$	0.107	0.118	0.041	0.052	0.027
$F_{\beta}^{\omega} \uparrow$	0.368	0.247	0.713	0.625	0.798
$E_{\phi} \uparrow$	0.678	0.669	0.872	0.831	0.926
$S_{\alpha} \uparrow$	0.644	0.621	0.798	0.743	0.853

(c) Cross-Scale Path Search

(d) Fusion Head

Table 2: Ablation studies of (a) Dual-Stream Frequency Modeling, (b) Operation Space \mathcal{O} , (c) Cross-Scale Path Search, (d) Fusion Head.

improvement is primarily driven by *NAS-discovered routing structure and operator placement*, rather than merely training or hyperparameter tuning.

Fusion head design. Concat+1×1 leaves cross-stream redundancy and Hamburger [75] adapts poorly to camouflage (Table 2d). Our low-rank *Soft-VQ* decoder (best at $r=32$) improves all metrics via compact embeddings and soft quantization that preserve fine details.

5 Conclusion

We presented CamoNAS, a NAS framework for camouflaged object detection that jointly searches cell-level operators and network-level multi-resolution routing while pairing an RGB stream with a learnable wavelet-based frequency stream and a lightweight low-rank fusion head. This task-aligned search yields compact topologies that sharpen boundaries, suppress background distractions, and generalize across diverse camouflage patterns. Empirically, CamoNAS shows strong performance on four COD benchmarks, consistently outperforming recent methods in our evaluations. These results demonstrate that automated, COD-aware architecture design is a principled alternative to hand-designed pipelines. Future work will enlarge the search space to enable *searchable* mid-level RGB–frequency coupling at intermediate stages (e.g., 1/8 and 1/16), so that the two streams can interact during feature formation rather than only at the final fusion head, and we will explore transfer to related dense prediction tasks.

References

- [1] Fan, D.-P., Ji, G.-P., Cheng, M.-M., Shao, L.: Concealed object detection. *IEEE transactions on pattern analysis and machine intelligence* **44**(10), 6024–6042 (2021)
- [2] Fan, D.-P., Ji, G.-P., Sun, G., Cheng, M.-M., Shen, J., Shao, L.: Camouflaged object detection. In: *CVPR*, pp. 2777–2787 (2020)

- [3] Yang, F., Zhai, Q., Li, X., Huang, R., Luo, A., Cheng, H., Fan, D.-P.: Uncertainty-guided transformer reasoning for camouflaged object detection. In: ICCV, pp. 4146–4155 (2021)
- [4] Fan, D.-P., Ji, G.-P., Zhou, T., Chen, G., Fu, H., Shen, J., Shao, L.: Pranel: Parallel reverse attention network for polyp segmentation. In: MICCAI, pp. 263–273 (2020). Springer
- [5] Zhang, R., Li, G., Li, Z., Cui, S., Qian, D., Yu, Y.: Adaptive context selection for polyp segmentation. In: MICCAI, pp. 253–262 (2020). Springer
- [6] Mei, H., Yang, X., Wang, Y., Liu, Y., He, S., Zhang, Q., Wei, X., Lau, R.W.: Don't hit me! glass detection in real-world scenes. In: CVPR, pp. 3687–3696 (2020)
- [7] Xie, E., Wang, W., Wang, W., Ding, M., Shen, C., Luo, P.: Segmenting transparent objects in the wild. In: ECCV (2020). Springer
- [8] Zhang, M., Xu, S., Piao, Y., Shi, D., Lin, S., Lu, H.: Preynet: Preying on camouflaged objects. In: ACM MM, pp. 5323–5332 (2022)
- [9] Mei, H., Ji, G.-P., Wei, Z., Yang, X., Wei, X., Fan, D.-P.: Camouflaged object segmentation with distraction mining. In: Proceedings of the IEEE/CVF Conference on Computer Vision and Pattern Recognition, pp. 8772–8781 (2021)
- [10] Pang, Y., Zhao, X., Xiang, T.-Z., Zhang, L., Lu, H.: Zoom in and out: A mixed-scale triplet network for camouflaged object detection. In: Proceedings of the IEEE/CVF Conference on Computer Vision and Pattern Recognition, pp. 2160–2170 (2022)
- [11] Cheng, A., Wu, S., Liu, X., Lu, H.: Enhancing concealed object detection in active thz security images with adaptation-yolo. *Scientific Reports* **15**(1), 2735 (2025)
- [12] Kowalski, M., Mierzejewski, K., Pałys, T.: Bi-spectral concealed object detection with attention-based fusion of passive thermal infrared and terahertz imaging. *Engineering Applications of Artificial Intelligence* **158**, 111462 (2025)
- [13] Liu, Z., Zhang, Z., Tan, Y., Wu, W.: Boosting camouflaged object detection with dual-task interactive transformer. In: 2022 26th International Conference on Pattern Recognition (ICPR), pp. 140–146 (2022). IEEE
- [14] Zhong, Y., Li, B., Tang, L., Kuang, S., Wu, S., Ding, S.: Detecting camouflaged object in frequency domain. In: CVPR, pp. 4504–4513 (2022)
- [15] He, C., Li, K., Zhang, Y., Tang, L., Zhang, Y., Guo, Z., Li, X.: Camouflaged object detection with feature decomposition and edge reconstruction. In: CVPR (2023)
- [16] Zhai, Q., Li, X., Yang, F., Chen, C., Cheng, H., Fan, D.-P.: Mutual graph learning

- for camouflaged object detection. In: CVPR, pp. 12997–13007 (2021)
- [17] Sun, Y., Wang, S., Chen, C., Xiang, T.-Z.: Boundary-guided camouflaged object detection. arXiv preprint arXiv:2207.00794 (2022)
- [18] Zhai, W., Cao, Y., Zhang, J., Zha, Z.-J.: Exploring figure-ground assignment mechanism in perceptual organization. In: NIPS, vol. 35 (2022)
- [19] Lv, Y., Zhang, J., Dai, Y., Li, A., Liu, B., Barnes, N., Fan, D.-P.: Simultaneously localize, segment and rank the camouflaged objects. In: CVPR, pp. 11591–11601 (2021)
- [20] Jia, Q., Yao, S., Liu, Y., Fan, X., Liu, R., Luo, Z.: Segment, magnify and reiterate: Detecting camouflaged objects the hard way. In: CVPR, pp. 4713–4722 (2022)
- [21] Zhu, H., Li, P., Xie, H., Yan, X., Liang, D., Chen, D., Wei, M., Qin, J.: I can find you! boundary-guided separated attention network for camouflaged object detection. In: AAAI, vol. 36, pp. 3608–3616 (2022)
- [22] Elsken, T., Metzen, J.H., Hutter, F.: Neural architecture search: A survey. *Journal of Machine Learning Research* **20**(55), 1–21 (2019)
- [23] Zoph, B., Le, Q.V.: Neural architecture search with reinforcement learning. arXiv preprint arXiv:1611.01578 (2016)
- [24] Zoph, B., Vasudevan, V., Shlens, J., Le, Q.V.: Learning transferable architectures for scalable image recognition. In: Proceedings of the IEEE Conference on Computer Vision and Pattern Recognition, pp. 8697–8710 (2018)
- [25] Liu, C., Zoph, B., Neumann, M., Shlens, J., Hua, W., Li, L.-J., Fei-Fei, L., Yuille, A., Huang, J., Murphy, K.: Progressive neural architecture search. In: Proceedings of the European Conference on Computer Vision (ECCV), pp. 19–34 (2018)
- [26] Real, E., Aggarwal, A., Huang, Y., Le, Q.V.: Regularized evolution for image classifier architecture search. In: Proceedings of the Aaai Conference on Artificial Intelligence, vol. 33, pp. 4780–4789 (2019)
- [27] Pham, H., Guan, M., Zoph, B., Le, Q., Dean, J.: Efficient neural architecture search via parameters sharing. In: International Conference on Machine Learning, pp. 4095–4104 (2018). PMLR
- [28] Liu, C., Chen, L.-C., Schroff, F., Adam, H., Hua, W., Yuille, A.L., Fei-Fei, L.: Auto-deeplab: Hierarchical neural architecture search for semantic image segmentation. In: Proceedings of the IEEE/CVF Conference on Computer Vision and Pattern Recognition, pp. 82–92 (2019)
- [29] Zhang, Y., Qiu, Z., Liu, J., Yao, T., Liu, D., Mei, T.: Customizable architecture search for semantic segmentation. In: Proceedings of the IEEE/CVF Conference

- on Computer Vision and Pattern Recognition, pp. 11641–11650 (2019)
- [30] Nekrasov, V., Chen, H., Shen, C., Reid, I.: Fast neural architecture search of compact semantic segmentation models via auxiliary cells. In: Proceedings of the IEEE/CVF Conference on Computer Vision and Pattern Recognition, pp. 9126–9135 (2019)
 - [31] Lin, P., Sun, P., Cheng, G., Xie, S., Li, X., Shi, J.: Graph-guided architecture search for real-time semantic segmentation. In: Proceedings of the IEEE/CVF Conference on Computer Vision and Pattern Recognition, pp. 4203–4212 (2020)
 - [32] Liu, H., Simonyan, K., Yang, Y.: Darts: Differentiable architecture search. arXiv preprint arXiv:1806.09055 (2018)
 - [33] Li, X., Fu, K., Zhao, Q.: Camouflaged object detection via neural architecture search. In: ICASSP 2025-2025 IEEE International Conference on Acoustics, Speech and Signal Processing (ICASSP), pp. 1–5 (2025). IEEE
 - [34] Liang, Y., Qin, G., Sun, M., Wang, X., Yan, J., Zhang, Z.: A systematic review of image-level camouflaged object detection with deep learning. *Neurocomputing* **566**, 127050 (2024)
 - [35] Cong, R., Sun, M., Zhang, S., Zhou, X., Zhang, W., Zhao, Y.: Frequency perception network for camouflaged object detection. In: Proceedings of the 31st ACM International Conference on Multimedia, pp. 1179–1189 (2023)
 - [36] Xie, C., Xia, C., Yu, T., Li, J.: Frequency representation integration for camouflaged object detection. In: Proceedings of the 31st ACM International Conference on Multimedia, pp. 1789–1797 (2023)
 - [37] Zhou, X., Yang, C., Zhao, H., Yu, W.: Low-rank modeling and its applications in image analysis. *ACM Computing Surveys (CSUR)* **47**(2), 1–33 (2014)
 - [38] Bi, H., Zhang, C., Wang, K., Tong, J., Zheng, F.: Rethinking camouflaged object detection: Models and datasets. *IEEE transactions on circuits and systems for video technology* **32**(9), 5708–5724 (2021)
 - [39] Mondal, A., Ghosh, S., Ghosh, A.: Partially camouflaged object tracking using modified probabilistic neural network and fuzzy energy based active contour. *International Journal of Computer Vision* **122**(1), 116–148 (2017)
 - [40] Li, S., Florencio, D., Li, W., Zhao, Y., Cook, C.: A fusion framework for camouflaged moving foreground detection in the wavelet domain. *IEEE Transactions on Image Processing* **27**(8), 3918–3930 (2018)
 - [41] Le, T.-N., Nguyen, T.V., Nie, Z., Tran, M.-T., Sugimoto, A.: Anabran network for camouflaged object segmentation. *Computer vision and image understanding*

- [42] Yin, B., Zhang, X., Fan, D.-P., Jiao, S., Cheng, M.-M., Van Gool, L., Hou, Q.: Camoformer: Masked separable attention for camouflaged object detection. *IEEE Transactions on Pattern Analysis and Machine Intelligence* (2024)
- [43] Yue, G., Jiao, G., Li, C., Xiang, J.: When cnn meet with vit: decision-level feature fusion for camouflaged object detection. *The Visual Computer* **41**(6), 3957–3972 (2025)
- [44] Ge, Y., Ren, J., Zhang, C., He, M., Bi, H., Zhang, Q.: Feature-aware and iterative refinement network for camouflaged object detection. *The Visual Computer* **41**(7), 4741–4758 (2025)
- [45] Skurowski, P., Abdulameer, H., Błaszczuk, J., Depta, T., Kornacki, A., Koziel, P.: Animal camouflage analysis: Chameleon database. Unpublished manuscript **2**(6), 7 (2018)
- [46] Lin, J., He, Z., Lau, R.W.: Rich context aggregation with reflection prior for glass surface detection. In: *CVPR*, pp. 13415–13424 (2021)
- [47] Ronneberger, O., Fischer, P., Brox, T.: U-net: Convolutional networks for biomedical image segmentation. In: *International Conference on Medical Image Computing and Computer-assisted Intervention*, pp. 234–241 (2015). Springer
- [48] Chen, L.-C., Papandreou, G., Kokkinos, I., Murphy, K., Yuille, A.L.: Deeplab: Semantic image segmentation with deep convolutional nets, atrous convolution, and fully connected crfs. *IEEE transactions on pattern analysis and machine intelligence* **40**(4), 834–848 (2017)
- [49] Kirillov, A., Wu, Y., He, K., Girshick, R.: Pointrend: Image segmentation as rendering. In: *Proceedings of the IEEE/CVF Conference on Computer Vision and Pattern Recognition*, pp. 9799–9808 (2020)
- [50] Lin, T.-Y., Dollár, P., Girshick, R., He, K., Hariharan, B., Belongie, S.: Feature pyramid networks for object detection. In: *Proceedings of the IEEE Conference on Computer Vision and Pattern Recognition*, pp. 2117–2125 (2017)
- [51] Zhang, M., Tian, X.: Transformer architecture based on mutual attention for image-anomaly detection. *Virtual Reality & Intelligent Hardware* **5**(1), 57–67 (2023) <https://doi.org/10.1016/j.vrih.2022.07.006>
- [52] Lin, C., Zou, C., Xu, H.: Snet: A dual-branch network for strong noisy image denoising based on swin transformer and convnext. *Computer Animation and Virtual Worlds* **36**(3), 70030 (2025) <https://doi.org/10.1002/cav.70030>
- [53] Zhang, M., Zhou, J., Miao, T., Zhao, Y., Si, X., Zhang, J.: Joint-learning: A robust

- segmentation method for 3d point clouds under label noise. *Computer Animation and Virtual Worlds* **36**(3), 70038 (2025) <https://doi.org/10.1002/cav.70038>
- [54] Yao, L., Xu, H., Zhang, W., Liang, X., Li, Z.: Sm-nas: Structural-to-modular neural architecture search for object detection. In: *Proceedings of the AAAI Conference on Artificial Intelligence*, vol. 34, pp. 12661–12668 (2020)
- [55] Chen, Y., Yang, T., Zhang, X., Meng, G., Xiao, X., Sun, J.: Detnas: Backbone search for object detection. *Advances in neural information processing systems* **32** (2019)
- [56] Guo, J., Han, K., Wang, Y., Zhang, C., Yang, Z., Wu, H., Chen, X., Xu, C.: Hit-detector: Hierarchical trinity architecture search for object detection. In: *Proceedings of the IEEE/CVF Conference on Computer Vision and Pattern Recognition*, pp. 11405–11414 (2020)
- [57] Wang, N., Gao, Y., Chen, H., Wang, P., Tian, Z., Shen, C., Zhang, Y.: Nas-fcos: Fast neural architecture search for object detection. In: *Proceedings of the IEEE/CVF Conference on Computer Vision and Pattern Recognition*, pp. 11943–11951 (2020)
- [58] Real, E., Moore, S., Selle, A., Saxena, S., Suematsu, Y.L., Tan, J., Le, Q.V., Kurakin, A.: Large-scale evolution of image classifiers. In: *International Conference on Machine Learning*, pp. 2902–2911 (2017). PMLR
- [59] Xu, Y., Xie, L., Zhang, X., Chen, X., Qi, G.-J., Tian, Q., Xiong, H.: Pc-darts: Partial channel connections for memory-efficient architecture search. *arXiv preprint arXiv:1907.05737* (2019)
- [60] Chen, X., Xie, L., Wu, J., Tian, Q.: Progressive differentiable architecture search: Bridging the depth gap between search and evaluation. In: *Proceedings of the IEEE/CVF International Conference on Computer Vision*, pp. 1294–1303 (2019)
- [61] Chu, X., Wang, X., Zhang, B., Lu, S., Wei, X., Yan, J.: Darts-: robustly stepping out of performance collapse without indicators. *arXiv preprint arXiv:2009.01027* (2020)
- [62] Chen, Z., Qiu, G., Li, P., Zhu, L., Yang, X., Sheng, B.: Mngnas: Distilling adaptive combination of multiple searched networks for one-shot neural architecture search. *IEEE Transactions on Pattern Analysis and Machine Intelligence* **45**(11), 13489–13508 (2023) <https://doi.org/10.1109/TPAMI.2023.3293885>
- [63] Ghiasi, G., Lin, T.-Y., Le, Q.V.: Nas-fpn: Learning scalable feature pyramid architecture for object detection. In: *Proceedings of the IEEE/CVF Conference on Computer Vision and Pattern Recognition*, pp. 7036–7045 (2019)
- [64] Tan, M., Chen, B., Pang, R., Vasudevan, V., Sandler, M., Howard, A., Le, Q.V.:

- Mnasnet: Platform-aware neural architecture search for mobile. In: Proceedings of the IEEE/CVF Conference on Computer Vision and Pattern Recognition, pp. 2820–2828 (2019)
- [65] Tan, M., Pang, R., Le, Q.V.: Efficientdet: Scalable and efficient object detection. In: Proceedings of the IEEE/CVF Conference on Computer Vision and Pattern Recognition, pp. 10781–10790 (2020)
- [66] Cai, H., Zhu, L., Han, S.: Proxylessnas: Direct neural architecture search on target task and hardware. arXiv preprint arXiv:1812.00332 (2018)
- [67] Lin, X., Sun, S., Huang, W., Sheng, B., Li, P., Feng, D.D.: Eapt: Efficient attention pyramid transformer for image processing. *IEEE Transactions on Multimedia* **25**, 50–61 (2023) <https://doi.org/10.1109/TMM.2021.3120873>
- [68] Liu, C., Chen, L.-C., Schroff, F., Adam, H., Hua, W., Yuille, A.L., Fei-Fei, L.: Auto-deeplab: Hierarchical neural architecture search for semantic image segmentation. In: Proceedings of the IEEE/CVF Conference on Computer Vision and Pattern Recognition, pp. 82–92 (2019)
- [69] Cheng, X., Zhong, Y., Harandi, M., Dai, Y., Chang, X., Li, H., Drummond, T., Ge, Z.: Hierarchical neural architecture search for deep stereo matching. *Advances in neural information processing systems* **33**, 22158–22169 (2020)
- [70] Na, B., Mok, J., Park, S., Lee, D., Choe, H., Yoon, S.: Autosnn: Towards energy-efficient spiking neural networks. In: International Conference on Machine Learning, pp. 16253–16269 (2022). PMLR
- [71] Qin, X., Zhang, Z., Huang, C., Gao, C., Dehghan, M., Jagersand, M.: Basnet: Boundary-aware salient object detection. In: Proceedings of the IEEE/CVF Conference on Computer Vision and Pattern Recognition, pp. 7479–7489 (2019)
- [72] Wei, J., Wang, S., Huang, Q.: F³net: fusion, feedback and focus for salient object detection. In: Proceedings of the AAAI Conference on Artificial Intelligence, vol. 34, pp. 12321–12328 (2020)
- [73] Huang, Z., Zhang, Z., Lan, C., Zha, Z.-J., Lu, Y., Guo, B.: Adaptive frequency filters as efficient global token mixers. In: Proceedings of the IEEE/CVF International Conference on Computer Vision, pp. 6049–6059 (2023)
- [74] He, S., Lin, G., Li, T., Chen, Y.: Frequency-domain fusion transformer for image inpainting. arXiv preprint arXiv:2506.18437 (2025)
- [75] Geng, Z., Guo, M.-H., Chen, H., Li, X., Wei, K., Lin, Z.: Is attention better than matrix decomposition? arXiv preprint arXiv:2109.04553 (2021)
- [76] Kirillov, A., Mintun, E., Ravi, N., Mao, H., Rolland, C., Gustafson, L., Xiao, T.,

Whitehead, S., Berg, A.C., Lo, W.-Y., et al.: Segment anything. arXiv preprint arXiv:2304.02643 (2023)

- [77] Li, A., Zhang, J., Lv, Y., Liu, B., Zhang, T., Dai, Y.: Uncertainty-aware joint salient object and camouflaged object detection. In: Proceedings of the IEEE/CVF Conference on Computer Vision and Pattern Recognition, pp. 10071–10081 (2021)
- [78] Ji, G.-P., Fan, D.-P., Chou, Y.-C., Dai, D., Liniger, A., Van Gool, L.: Deep gradient learning for efficient camouflaged object detection. *Machine Intelligence Research* **20**(1), 92–108 (2023)
- [79] Wu, Z., Paudel, D.P., Fan, D.-P., Wang, J., Wang, S., Demonceaux, C., Timofte, R., Van Gool, L.: Source-free depth for object pop-out. In: Proceedings of the IEEE/CVF International Conference on Computer Vision, pp. 1032–1042 (2023)
- [80] He, R., Dong, Q., Lin, J., Lau, R.W.: Weakly-supervised camouflaged object detection with scribble annotations. *AAAI* (2023)
- [81] He, C., Li, K., Zhang, Y., Xu, G., Tang, L., Zhang, Y., Guo, Z., Li, X.: Weakly-supervised concealed object segmentation with sam-based pseudo labeling and multi-scale feature grouping. *Advances in Neural Information Processing Systems* **36**, 30726–30737 (2023)
- [82] He, C., Li, K., Zhang, Y., Zhang, Y., Guo, Z., Li, X., Danelljan, M., Yu, F.: Strategic preys make acute predators: Enhancing camouflaged object detectors by generating camouflaged objects. arXiv preprint arXiv:2308.03166 (2023)
- [83] Zhou, X., Wu, Z., Cong, R.: Decoupling and integration network for camouflaged object detection. *IEEE Transactions on Multimedia* **26**, 7114–7129 (2024)
- [84] Pang, Y., Zhao, X., Xiang, T.-Z., Zhang, L., Lu, H.: Zoomnext: A unified collaborative pyramid network for camouflaged object detection. *IEEE transactions on pattern analysis and machine intelligence* **46**(12), 9205–9220 (2024)
- [85] Hu, J., Lin, J., Gong, S., Cai, W.: Relax image-specific prompt requirement in sam: A single generic prompt for segmenting camouflaged objects. In: Proceedings of the AAAI Conference on Artificial Intelligence, vol. 38, pp. 12511–12518 (2024)
- [86] Yan, W., Chen, L., Kou, H., Zhang, S., Zhang, Y., Cao, L.: Ucod-dpl: Unsupervised camouflaged object detection via dynamic pseudo-label learning. In: Proceedings of the Computer Vision and Pattern Recognition Conference, pp. 30365–30375 (2025)
- [87] Gupta, A., Jerripothula, K.R., Tillo, T.: Circod: Co-saliency inspired referring camouflaged object discovery. In: 2025 IEEE/CVF Winter Conference on Applications of Computer Vision (WACV), pp. 8313–8323 (2025). IEEE